catalysts

MDPI

Article

Hg^0 Removal by V_2O_5 Modified Palygorskite in Simulated Flue Gas at Low Temperature

Junwei Wang [1], Huan Wang [1], Caihong Jiang [1], Xie Wang [1,*] and Jianli Zhang [2,*]

[1] College of Chemistry and Chemical Engineering, Anqing Normal University, Anqing 246011, China; wangjunweilotus@163.com (J.W.); xiaowanghenwasaiya@163.com (H.W.); jch177512@163.com (C.J.)
[2] State Key Laboratory of High-Efficiency Utilization of Coal and Green Chemical Engineering, Ningxia University, Yinchuan 750021, China
* Correspondence: anhuiss@sina.com (X.W.); zhangjl@nxu.edu.cn (J.Z.)

Abstract: The V_2O_5-modified palygorskite (V_2O_5/PG catalysts) were prepared and used for Hg^0 removal in simulated flue gas at low temperature. It was found that the V_2O_5/PG catalyst had excellent performance for Hg^0 removal at 150 °C. O_2 exhibited a positive effect on Hg^0 removal over V_2O_5/PG, while SO_2 and H_2O showed an inhibiting effect. However, Hg^0 removal efficiency showed a promotion trend in the presence of H_2O, SO_2, and O_2. The Brunauer–Emmett–Teller (BET) method, scanning electron microscopy (SEM), and X-ray photoelectron spectroscopy (XPS) were applied to characterize the physicochemical properties of the V_2O_5/PG catalyst. Mercury temperature-programmed desorption (Hg-TPD) experiments were also conducted to identify the mercury species adsorbed on the V_2O_5/PG catalyst, and the pathway of Hg^0 removal over V_2O_5/PG was also discussed. The used V_2O_5/PG catalyst after Hg^0 removal was regenerated, and its capability for Hg^0 removal can be completely recovered. The V_2O_5/PG-Re-300 °C catalyst showed excellent performance and good stability for Hg^0 removal after regeneration.

Keywords: Hg^0; V_2O_5/PG; palygorskite; catalytic oxidation; low temperature

check for updates

Citation: Wang, J.; Wang, H.; Jiang, C.; Wang, X.; Zhang, J. Hg^0 Removal by V_2O_5 Modified Palygorskite in Simulated Flue Gas at Low Temperature. *Catalysts* **2022**, *12*, 243. https://doi.org/10.3390/catal12020243

Academic Editor: Federica Menegazzo

Received: 20 January 2022
Accepted: 17 February 2022
Published: 21 February 2022

Publisher's Note: MDPI stays neutral with regard to jurisdictional claims in published maps and institutional affiliations.

Copyright: © 2022 by the authors. Licensee MDPI, Basel, Switzerland. This article is an open access article distributed under the terms and conditions of the Creative Commons Attribution (CC BY) license (https://creativecommons.org/licenses/by/4.0/).

1. Introduction

Mercury, as a trace toxic chemical, is harmful and threatening to people's health and the environment [1–3]. In China, about 38% of annual mercury emissions are from coal-fired power plants, which are regarded as the main anthropogenic source of mercury emissions [4–6]. Therefore, more and more attention has been paid to mercury emission control from coal-fired flue gas. To control mercury release, a series of environmental regulations and laws have been promulgated. The Minamata Convention on Mercury has been in effect since 16 August 2017, which means that reducing atmospheric mercury emissions has been a consensus-driven and compulsive goal of many countries around the world [7]. Moreover, the new Emission Standard of Air Pollutants for Thermal Power Plants in China has been executed, and explicitly stipulates that the emission limitation of mercury and its compounds in coal-fired flue gas is 30 $\mu g/m^3$ [8]. Therefore, the control situation of mercury in coal-fired flue gas is very serious. The urgent task is to develop and research effective and economical technology for mercury emissions in coal-fired power plants.

Generally, coal-fired flue gas mainly contains several components, including O_2 (3–7%) (v/v), moisture (8–10%) (v/v), SO_2 (100–3000 ppm), etc. [9,10]. Mercury in coal-fired flue gas mainly exists in three forms: oxidized mercury (Hg^{2+}), particulate mercury (Hg^p), and elemental mercury (Hg^0) [11,12]. Among them, wet flue gas desulfurization (WFGD) can effectively remove Hg^{2+} [13,14], and electrostatic precipitators (ESPs) or fabric filters (FFs) can easily capture Hg^p [15]. However, due to its high volatility, stability, and insolubility, Hg^0 is difficult to remove by existing air pollution control devices (APCDs) [16,17]. Therefore, researchers focus their efforts on controlling the emission of Hg^0 from flue gas.

Various methods have been studied and used to control Hg^0 emission, such as activated carbon injection (ACI) [18,19], catalytic oxidation, photochemical oxidation, and adsorption [20–22]. Among them, ACI technology is considered as the most effective Hg^0 control technology [23]. However, the large-scale industrial application of ACI technology is limited due to its high operation cost [24–26].

In recent years, the natural mineral has attracted the attention of researchers since the raw materials are abundant in reserves and are cost-effective [27,28]. Palygorskite (noted as PG), as a kind of natural magnesium aluminum silicate clay mineral, has a unique crystal structure, well-developed pores, high specific surface area, high adsorption ability, good cohesiveness and mechanical properties, low price, and can be used as a good catalyst carrier. However, few studies have been reported on Hg^0 removal by PG from flue gas at low temperature.

It is well known that V_2O_5-based selective catalytic reduction (SCR) catalysts are widely used for NO_x removal in coal-fired flue gas [29,30]. Meanwhile, it was also found that V_2O_5 exhibited high catalytic oxidation activity for Hg^0 and can effectively oxidize Hg^0 to Hg^{2+} [31–34]. However, V_2O_5-based SCR catalysts themselves have limited ability to adsorb the formed Hg^{2+} at high operating temperatures (300–450 °C), and the formed Hg^{2+} must be removed by the downstream WFGD unit [13]. Therefore, it is necessary to develop cost-effective and environmentally friendly technologies for Hg^0 control in coal-fired flue gas at low temperature.

In this work, palygorskite-supported V_2O_5 catalysts (V_2O_5/PG) were prepared and used to remove Hg^0 in simulated flue gas at low temperature (120–210 °C). The V_2O_5/PG catalysts were characterized by BET, SEM, XPS, and Hg-TPD. Moreover, the effects of V_2O_5 loading, temperature, flue gas components (SO_2, H_2O, and O_2), space velocity (GHSV), and the reaction pathways were also studied in the presence of SO_2. The regeneration of the used V_2O_5/PG catalyst after Hg^0 removal and reuse for Hg^0 removal were also studied.

2. Results and Discussion

2.1. Effect of Reaction Temperature

Figure 1 shows the effect of reaction temperature (120 °C, 150 °C, 180 °C, and 210 °C) on Hg^0 removal over $5V_2O_5$/PG catalyst. It can be seen that the initial E_{Hg} of $5V_2O_5$/PG reached 98% at 120 °C, and that it decreased gradually to 73.8% at 420 min. As the temperature increased from 150 °C to 180 °C and 210 °C, E_{Hg} decreased from 83.1%, 78.4%, and 52.5% at 420 min, respectively. Generally, adsorption becomes weaker at high temperature while oxidation will be enhanced. The difference of E_{Hg} at different temperatures may be due to the different effect extent of adsorption and oxidation at different temperatures [35]. The $5V_2O_5$/PG catalyst had the highest Hg^0 removal capability at 150 °C, which was much lower than the operating temperature of the V_2O_5-based SCR catalyst. Meanwhile, the V_2O_5/PG catalyst had much higher adsorption ability than that of V_2O_5-based SCR catalyst. Furthermore, the optimum reaction temperature (150 °C) was very close to the actual exhaust gas temperature of flue gas in a power plant, indicating that the V_2O_5/PG catalyst can be used to remove Hg^0 from flue gas without an extra heat supply.

2.2. Effect of V_2O_5 Loading

Figure 2 shows the effect of V_2O_5 loading on Hg^0 removal over V_2O_5/PG at 150 °C. Since it was found that a V_2O_5 loading range of 1% to 5% was favorable in our previous research, V_2O_5 loading (1% to 5%) was selected in this paper [36]. It can be seen that E_{Hg} of the PG carrier was very low, and that it decreased rapidly from 50% to 8.3% in 300 min. The E_{Hg} of the V_2O_5/PG was obviously higher than that of the PG, which was mainly due to the contribution of V_2O_5. V_2O_5, as the active site for Hg^0 oxidation, was of great importance in Hg^0 removal by V_2O_5/PG. It was found that lattice oxygen of V_2O_5 played a critical role in Hg^0 oxidation in our previous research, which was consumed in Hg^0 oxidation and can be subsequently replenished by gas-phase O_2 [35]. With the increase of V_2O_5 loading (1% to 5%), the E_{Hg} increased from 38.6% to 86.0% at 420 min. Since the

$5V_2O_5$/PG catalyst showed the best Hg^0 removal performance, $5V_2O_5$/PG was used in the following experiments.

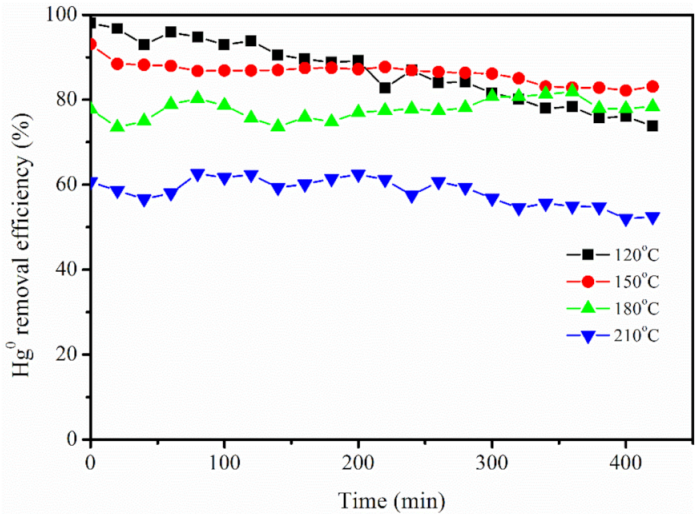

Figure 1. Effect of temperature on Hg^0 removal over $5V_2O_5$/PG (reaction conditions: O_2 = 8%, H_2O = 5%, SO_2 = 0.15%, N_2 as balance, $C_{Hg}{}^0$ = 240 μg/m^3, GHSV = 6000 h^{-1}, T = 120–210 °C).

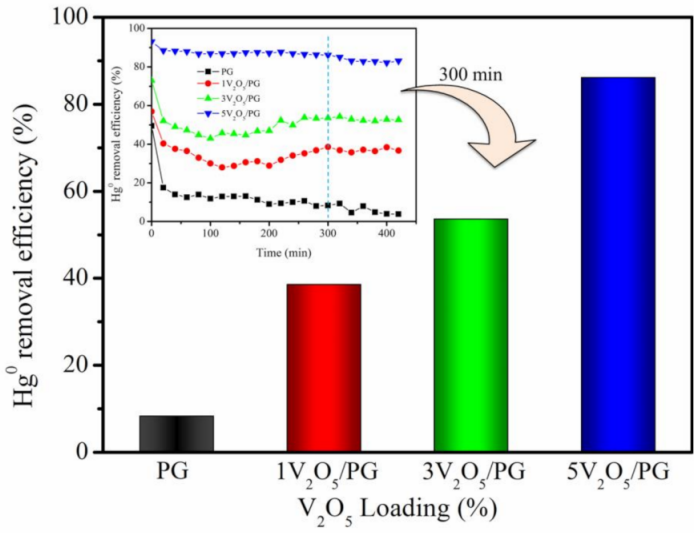

Figure 2. Effect of V_2O_5 loading on Hg^0 removal (reaction conditions: O_2 = 8%, H_2O = 5%, SO_2 = 0.15%, N_2 as balance, $C_{Hg}{}^0$ = 240 μg/m^3, GHSV = 6000 h^{-1}, T = 150 °C).

The specific surface areas and other pore parameters of the PG and V_2O_5/PG catalysts are summarized in Table 1. It can be seen that the BET surface area and total pore volume of the V_2O_5/PG catalyst are lower than those of the pure PG carrier. With the increase of the V_2O_5 loading, the BET area of the catalyst decreased obviously (from 151.4 m^2/g to 109.3 m^2/g). This may be due to the pores of the PG carrier being blocked by the active component of V_2O_5 and/or the sloughing of the PG skeleton during the calcination process, which led to the decrease of the BET area of the V_2O_5/PG catalyst. It is well known that a larger BET area can provide more reaction sites for the adsorption of Hg^0. However, the specific surface area of the V_2O_5/PG catalyst showed little effect on Hg^0 removal, i.e., the BET area was not the decisive factor affecting Hg^0 removal, while the oxidation activity of V_2O_5 played a critical role in Hg^0 removal. This was similar to the results reported in the literature [35].

Table 1. Properties of the PG and V_2O_5/PG catalysts.

Sample	BET Surface Area (m^2/g)	Average Pore Size (nm)	Total Pore Volume (cm^3/g)
PG	151.43	10.51	0.32
$1V_2O_5$/PG	139.91	10.67	0.30
$3V_2O_5$/PG	130.24	10.85	0.26
$5V_2O_5$/PG	109.31	11.04	0.21

Figure 3A,B shows the SEM morphology of $5V_2O_5$/PG. It can be seen that the V_2O_5/PG catalyst had a porous structure, which was conducive to the distribution of V_2O_5 on the surface of the PG carrier and the adsorption of Hg^0 on the surface of the V_2O_5/PG catalyst. The Lewis acid–base properties of the PG and V_2O_5/PG catalysts were analyzed and the detailed results are shown in the Supporting Information. The results showed that there were several different acid sites on the V_2O_5/PG catalyst surface, which were beneficial for Hg^0 adsorption on V_2O_5/PG.

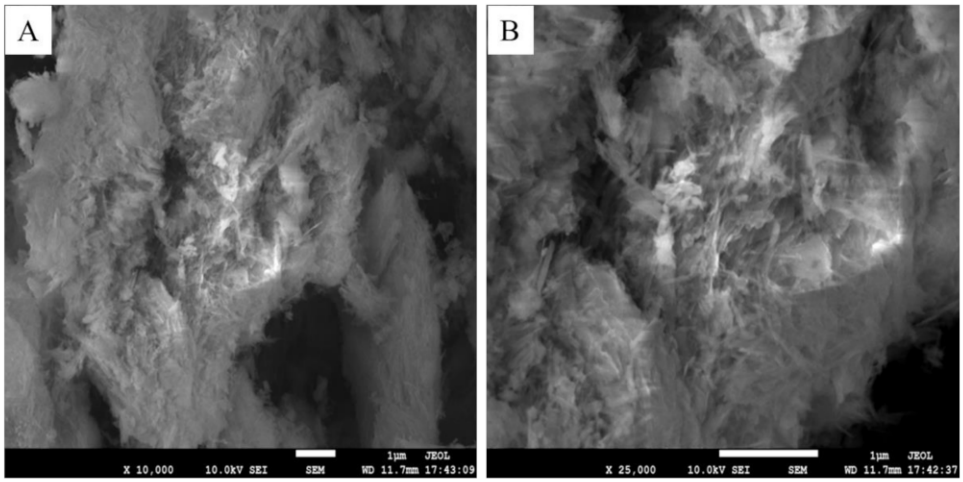

Figure 3. SEM morphology of $5V_2O_5$/PG (**A**): ×10,000; (**B**): ×25,000.

2.3. Effect of Flue Gas Components on Hg^0 Removal

Figure 4A shows the effects of flue gas components on Hg^0 removal over $5V_2O_5$/PG. It can be seen that the $5V_2O_5$/PG catalyst exhibited excellent Hg^0 removal capability (E_{Hg} = 90.9%) within 400 min in a N_2 atmosphere. However, after 0.15% SO_2 was introduced, an obviously inhibitive effect was observed, and the E_{Hg} decreased to 43.5%. A similar negative effect (E_{Hg} = 53.48%) was also observed by adding 5% H_2O into N_2. These may be due to the competitive adsorption of SO_2 (or H_2O) with Hg^0 on the surface of $5V_2O_5$/PG in a N_2 atmosphere, as well as the reaction of SO_2, H_2O, and V_2O_5 [18,35]. Adding 8% O_2 into the N_2 atmosphere promoted Hg^0 removal over V_2O_5/PG, and the E_{Hg} increased to 96.8%, indicating that O_2 played a positive role in Hg^0 removal. Since no Hg^0 oxidation by O_2 was measured in the gas phase, the effect of O_2 should be on V_2O_5, i.e., V_2O_5 was reduced to V^{4+} in Hg^0 oxidation and lost its oxidation activity, while O_2 can replenish O to the used V_2O_5 sites and resume its oxidation activity. This was consistent with SO_2 removal and Hg^0 oxidation over V_2O_5/AC catalysts in our previous research [37], and is similar to Hg^0 oxidation on metal oxide catalysts [38,39].

Figure 4B shows Hg^0 removal over $5V_2O_5$/PG in a complex atmosphere containing more components. As mentioned above (Figure 4A), E_{Hg} was 43.5% in N_2 + SO_2, and it decreased to 34.2% after adding 5% H_2O into N_2 + SO_2. However, after 8% O_2 was added into N_2 + SO_2 or N_2 + H_2O, the E_{Hg} increased to 72.4% and 77.4%, respectively. This suggested that O_2 played a critical role and could offset the negative effect of H_2O (or SO_2) on Hg^0 removal to a certain extent [18,40–42]. The E_{Hg} increased to 86.9% after

5% H_2O was added into N_2 + O_2 + SO_2, which may be due to the formation of SO_4^{2-}, which could react with Hg^0 [43–45]. $HgSO_4$ was formed, as shown in the following TPD experiment results.

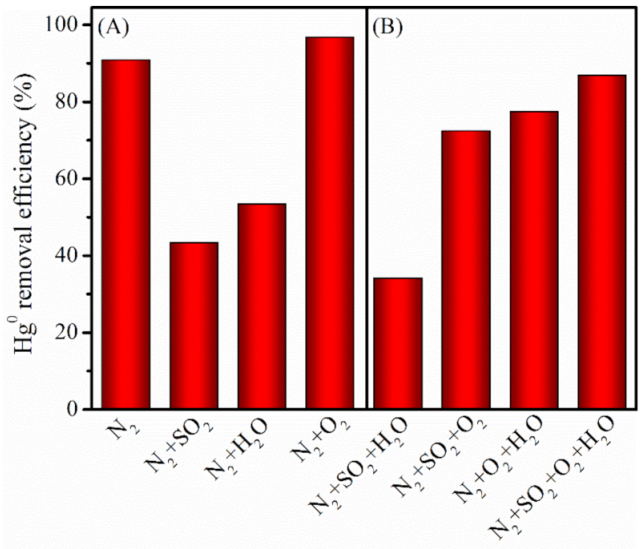

Figure 4. Effect of flue gas components on Hg^0 removal over $5V_2O_5/PG$ ((**A**) single component; (**B**) multi-components. reaction conditions: O_2 = 8%, H_2O = 5%, SO_2 = 0.15%, N_2 as balance, $C_{Hg}{}^0$ = 240 μg/m^3, GHSV = 6000 h^{-1}, T = 150 °C).

2.4. Effects of GHSV on Hg^0 Removal

The GHSV, as an important industrial parameter, can directly affect the contact time between the flue gas components and catalyst bed, and it has an important influence on the Hg^0 removal process. Figure 5 shows the results of Hg^0 removal by $5V_2O_5/PG$ at different GHSV (6000 h^{-1}, 10,000 h^{-1}, and 15,000 h^{-1}) at 150 °C. It can be seen that GHSV had an obvious effect on Hg^0 removal over $5V_2O_5/PG$. As the GHSV increased from 6000 h^{-1} to 15,000 h^{-1}, the E_{Hg} decreased from 86.9% to 57.9% in 400 min. The lower GHSV (6000 h^{-1}) is more beneficial for Hg^0 removal over $5V_2O_5/PG$. This may be due to the lower GHSV increasing the contact time of Hg^0 and $5V_2O_5/PG$ [35]. The $5V_2O_5/PG$ catalyst exhibited good Hg^0 removal activity at 6000 h^{-1}, which can match the actual GHSV of flue gas in a power plant and was suitable for mercury removal in power plants.

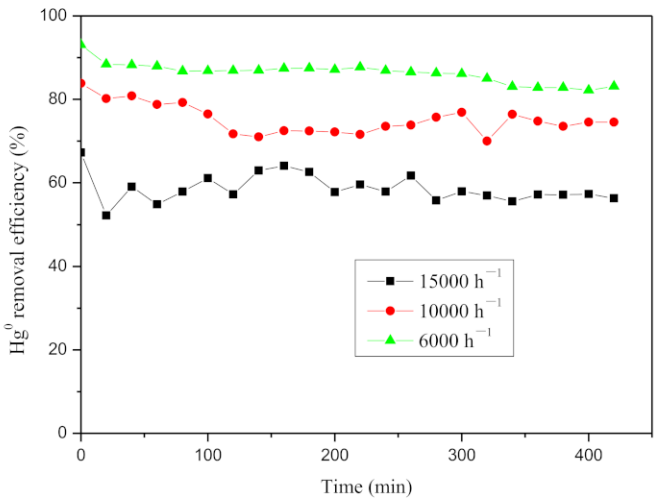

Figure 5. Effect of GHSV on Hg^0 removal over $5V_2O_5/PG$ (reaction conditions: O_2 = 8%, H_2O = 5%, SO_2 = 0.15%, N_2 as balance, $C_{Hg}{}^0$ = 240 μg/m^3, GHSV = 6000–15,000 h^{-1}, T = 150 °C).

2.5. The Pathway of Hg^0 Removal over V_2O_5/PG

The speciation of Hg adsorbed on the surface of V_2O_5/PG was characterized by XPS, and the results are shown in Figure 6. It can be seen that there was only one peak, at 102.90 eV, for the fresh $5V_2O_5$/PG, which could be attributed to Si 2p in the PG carrier. As for the spent $5V_2O_5$/PG after Hg^0 removal, two peaks were observed at 103.1 eV and 107.15 eV, respectively. The peak at 103.1 eV can be assigned to Si 2p of the PG carrier, while the peak at 107.15 eV was attributed to Hg^{2+} [24,28].

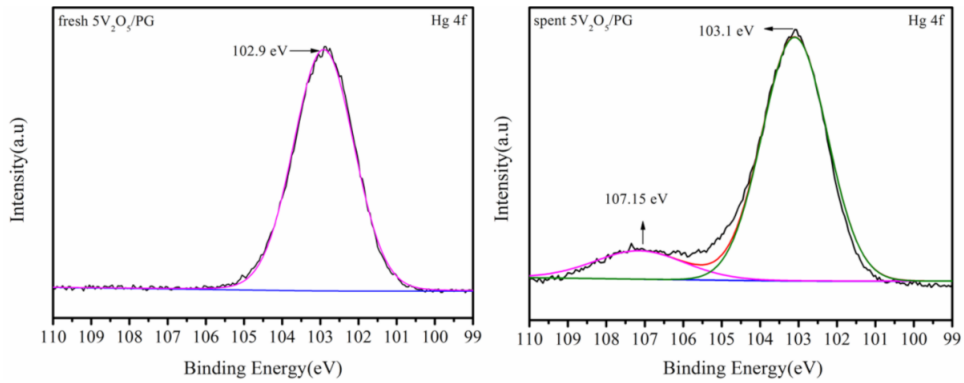

Figure 6. XPS of Hg 4f for fresh and spent V_2O_5/PG catalyst.

To further investigate the mercury species adsorbed over V_2O_5/PG, the experiments of Hg temperature-programmed desorption (Hg-TPD) were performed for the fresh and spent $5V_2O_5$/PG. As shown in Figure 7, it can be seen that there was no Hg release peak during the whole Hg-TPD process for the fresh $5V_2O_5$/PG sample. However, as for the spent $5V_2O_5$/PG sample, two Hg release peaks appeared at 240 °C and 495 °C, respectively. This indicated that there were two forms of mercury on the surface of the spent $5V_2O_5$/PG, which can be ascribed to HgO and $HgSO_4$ [46,47]; the relevant reactions may be described as follows, and the enthalpy change of adsorption and reactions were calculated in the Vienna ab initio simulation package (VASP 5.4.4) [48]:

$$Hg^0\ (gas) \rightarrow Hg^0\ (ad) \qquad (\triangle H = -18.337\ kJ/mol)$$

$$O_2\ (gas) \rightarrow O_2\ (ad) \qquad (\triangle H = -12.589\ kJ/mol)$$

$$SO_2\ (gas) \rightarrow SO_2\ (ad) \qquad (\triangle H = -33.545\ kJ/mol)$$

$$2Hg^0\ (ad) + O_2\ (ad) \rightarrow 2HgO\ (ad) \qquad (\triangle H = 147.448\ kJ/mol)$$

$$SO_2\ (ad) + O_2\ (ad) + Hg^0\ (ad) \rightarrow HgSO_4\ (ad) \qquad (\triangle H = -161.557\ kJ/mol)$$

Additionally, it can be seen that the Hg adsorbed on $5V_2O_5$/PG began to release at 150 °C, which could well explain the result of Figure 2 that the E_{Hg} decreased as the temperature was higher than 150 °C.

2.6. Regeneration of V_2O_5/PG Catalyst after Hg^0 Removal

The above results showed that the $5V_2O_5$/PG catalyst had an excellent Hg^0 removal capability at low temperature. To investigate the reusability of the $5V_2O_5$/PG catalyst, the $5V_2O_5$/PG after Hg^0 removal was regenerated and reused for Hg^0 removal again. Since the V_2O_5/PG catalyst was prepared by calcining at 300 °C in air, a regeneration temperature was chosen from 300 °C to 500 °C to resume its catalytic activity. The results of the PG, $5V_2O_5$/PG, $5V_2O_5$/PG-Re-300 °C, $5V_2O_5$/PG-Re-400 °C, and $5V_2O_5$/PG-Re-500 °C for Hg^0 removal are shown in Figure 8. It can be seen that, with the rise of regeneration temperature (from 300 °C to 500 °C), the E_{Hg} of $5V_2O_5$/PG-Re-x decreased obviously. $5V_2O_5$/PG-Re-300 °C showed the highest activity (E_{Hg} = 90.3%) at 420 min, even higher than that of the fresh $5V_2O_5$/PG catalyst (E_{Hg} = 83.1%). The E_{Hg} of $5V_2O_5$/PG-

Re-400 °C and $5V_2O_5$/PG-Re-500 °C were 66.7% and 46.8%, respectively. This may be due to the change of structure and chemical properties of $5V_2O_5$/PG during regeneration, which caused partial active sites loss on the surface of the $5V_2O_5$/PG catalyst at higher regeneration temperatures (400 °C and 500 °C) [36].

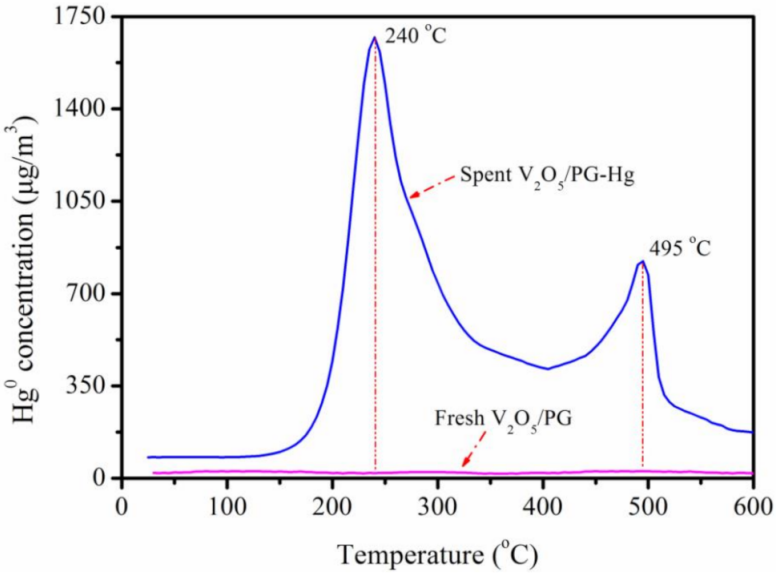

Figure 7. TPD profiles of fresh and spent $5V_2O_5$/PG (reaction conditions: T = 30–600 °C, N_2 = 200 mL/min, heating rate = 5 °C/min).

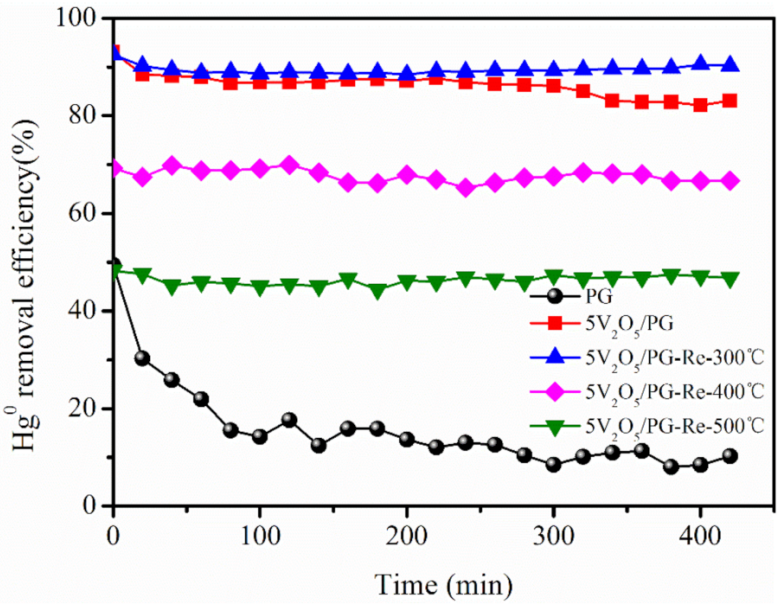

Figure 8. Comparison of Hg^0 removal over PG, $5V_2O_5$/PG, $5V_2O_5$/PG-Re-300 °C, $5V_2O_5$/PG-Re-400 °C, and $5V_2O_5$/PG-Re-500 °C (reaction condition: O_2 = 8%, H_2O = 5%, SO_2 = 0.15%, N_2 as balance, C_{Hg^0} = 240 μg/m^3, GHSV = 6000 h^{-1}, T = 150 °C).

3. Materials and Methods

3.1. Catalysts Preparation

The PG was mixed with distilled water in a certain proportion (1 g: 4–8 mL), dried at 110 °C for 6 h, then calcined at 300 °C for 6 h in air. The obtained PG samples were crushed and screened into a 40–60 mesh.

The xV_2O_5/PG catalysts (x is the mass fraction of V_2O_5 in the V_2O_5/PG catalyst, and x = 0–5 wt%) were prepared by impregnating PG particles with different V_2O_5 loadings,

which was similar to the V_2O_5/AC catalysts in our previous research [36]., Briefly, the PG particles are impregnated in ammonium metavanadate solution with the required concentration for 1 h, dried at 60 °C for 5 h, then 110 °C for 8 h. Finally, the samples were calcined at 300 °C for 4 h in air.

3.2. Catalytic Activity Evaluation of V_2O_5/PG

The catalytic activity of the V_2O_5/PG catalyst for Hg^0 removal was tested in a bench-scale fixed-bed reactor; a detailed description of the experimental schematic is in Figure 9. The Hg^0 removal activity evaluation device system mainly includes simulated flue gas, a programmed temperature controller, a fixed-bed reactor, an online mercury analyzer and a tail gas treatment cleaner. A total of 0.5 g V_2O_5/PG was loaded into the quartz tube. The simulated flue gas includes 8% O_2, 0.15% SO_2, 5% H_2O and balance N_2, and was controlled by a mass flowmeter. The GHSV was approximately 6000 h^{-1}. The temperature (120–210 °C) was controlled by a digital temperature controller. The Hg^0 vapor was produced from a mercury permeation tube (VICI Metronics) and carried out by N_2 with a constant flow rate. Hg^0 concentration was detected by an online RA-915M Mercury Analyzer (Lumex Co, Ltd., St. Petersburg, Russia). Finally, the tail gas was treated by a device equipped with activated carbon.

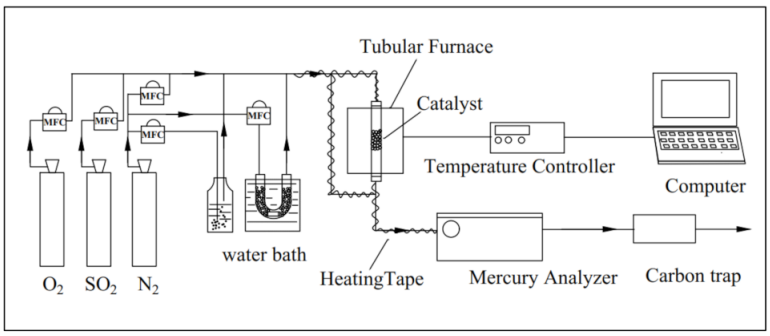

Figure 9. Schematic diagram of the fixed-bed reactor for Hg^0 removal by V_2O_5/PG.

The Hg^0 removal efficiency (E_{Hg}) was defined as follows:

$$E_{Hg}(\%) = \frac{C_0 - C_1}{C_0} \times 100\ \% \quad (1)$$

where C_0 and C_1 represent the Hg^0 concentration (μg/m^3) at the inlet and outlet of the reactor, respectively.

3.3. Characterization

The N_2 adsorption–desorption tests were carried out by an Autosorb-iQ analyzer (Quantachrome, Boynton Beach, FL, USA). The specific surface areas were calculated by the Brunauer–Emmett–Teller (BET) method, the pore structure parameters were analyzed by the Barrett–Joyner–Halenda (BJH) method.

The morphologies of the V_2O_5/PG samples were observed, which was performed on a scanning electron microscope (SEM) (JSM-7001F, JEOL, Akishima City, Japan).

The X-ray photoelectron spectroscopy (XPS) analysis was performed on an ESCALAB 250Xi spectrometer (Thermo Fisher, Waltham, MA, USA) using an Al Kα X-ray source at room temperature. All binding energies (BE) were adjusted with the C 1s binding energy value of 284.6 eV.

The Hg temperature-programmed desorption (Hg-TPD) experiments were conducted in a quartz tube reactor using a 0.1 g sample in N_2 (200 mL/min). The sample was firstly used to remove Hg^0 at 150 °C for 6 h, then swept with N_2 at 150 °C for 2 h, and finally, heated from 30 °C to 600 °C with a heating rate of 5 °C/min. The outlet gas from the reactor was introduced into a KBH_4 solution to reduce the possibly existing Hg^{2+} to Hg^0. The Hg^0

concentration in the effluent gas after the KBH_4 solution was continuously measured by an on-line mercury analyzer (RA-915M, Lumex, St. Petersburg, Russia).

4. Conclusions

The V_2O_5/PG catalyst had excellent Hg^0 removal capability, which was mainly due to the V_2O_5/PG catalyst combined with the adsorption ability of PG and the catalytic oxidation activity of V_2O_5. Hg^0 was oxidized to form HgO and $HgSO_4$, and then adsorbed on the V_2O_5/PG catalyst. The E_{Hg} of the V_2O_5/PG catalyst increased with the increase of V_2O_5 loading, and the $5V_2O_5$/PG catalyst showed the highest E_{Hg} at 150 °C. O_2 exhibited a promoting effect on Hg^0 removal, while SO_2 and H_2O showed an obvious inhibitory effect. However, when O_2, H_2O, and SO_2 were added together, the E_{Hg} showed a promoting trend. The used V_2O_5/PG catalyst after Hg^0 removal can be regenerated and its capability for Hg^0 removal can be completely recovered, and the V_2O_5/PG-Re-300 °C catalyst showed excellent performance and good stability for Hg^0 removal after regeneration.

Author Contributions: Conceptualization, J.W. and X.W.; methodology, J.W.; validation, H.W., C.J. and J.W.; formal analysis, H.W.; investigation, H.W.; data curation, C.J.; writing—original draft preparation, J.W.; writing—review and editing, J.Z.; visualization, H.W.; supervision, J.W.; project administration, X.W.; funding acquisition, J.Z. All authors have read and agreed to the published version of the manuscript.

Funding: This research was funded by the National Natural Science Foundation of China (21203003, 51404014), Foundation of State Key Laboratory of High-efficiency Utilization of Coal and Green Chemical Engineering (2020-KF-28) and Anhui Provincial Discipline (Professional) Top Talent Academic Funding Project (gxbjZD2021062).

Data Availability Statement: Not available.

Conflicts of Interest: The authors declare no conflict of interest.

References

1. Horowitz, H.M.; Jacob, D.J.; Amos, H.M.; Streets, D.G.; Sunderland, E.M. Historical mercury releases from commercial products: Global environmental implications. *Environ. Sci. Technol.* **2014**, *48*, 10242–10250. [CrossRef] [PubMed]
2. Nriagu, J.O.; Pacyna, J.M. Quantitative assessment of worldwide contamination of air, water and soils by trace metals. *Nature* **1988**, *333*, 134–139. [CrossRef] [PubMed]
3. Gao, Y.S.; Zhang, Z.; Wu, J.W.; Duan, L.H.; Umar, A.; Sun, L.H. A critical review on the heterogeneous catalytic oxidation of elemental mercury in flue gases. *Environ. Sci. Technol.* **2013**, *47*, 10813–10823. [CrossRef] [PubMed]
4. Kocman, D.; Horvat, M.; Pirrone, N.; Cinnirella, S. Contribution of contaminated sites to the global mercury budget. *Environ. Res.* **2013**, *125*, 160–170. [CrossRef] [PubMed]
5. Li, H.L.; Wu, C.Y.; Li, Y.; Li, L.Q.; Zhao, Y.C.; Zhang, J.Y. Impact of SO_2 on elemental mercury oxidation over CeO_2-TiO_2 catalyst. *Chem. Eng. J.* **2013**, *219*, 319–326. [CrossRef]
6. Streets, D.G.; Hao, J.M.; Wu, Y.; Jiang, J.K.; Chan, M.; Tian, H.Z. Anthropogenic mercury emissions in China. *Atmos. Environ.* **2005**, *39*, 7789–7806. [CrossRef]
7. Wu, Q.R.; Wang, S.X.; Liu, K.Y.; Li, G.L.; Hao, J.M. Emission-limit-oriented strategy to control atmospheric mercury emissions in coal-fired power plants toward the implementation of the Minamata Convention. *Environ. Sci. Technol.* **2018**, *52*, 11087–11093. [CrossRef]
8. Zhao, Y.; Ma, X.Y.; Xu, P.Y.; Wang, H.; Liu, Y.C.; He, A.E. Elemental mercury removal from flue gas by $CoFe_2O_4$ catalyzed peroxymonosulfate. *J. Hazard. Mater.* **2018**, *341*, 228–237. [CrossRef]
9. Liu, W.; Vidic, R.D.; Brown, T.D. Impact of flue gas conditions on mercury uptake by sulfur-impregnated activated carbon. *Environ. Sci. Technol.* **2000**, *34*, 154–159. [CrossRef]
10. Luo, J.J.; Zhang, L.D.; Huang, H.W.; Zhang, J.R. Effects of flue gas components and fly ash on mercury oxidation. *J. Univ. Sci. Technol. Beijing* **2011**, *33*, 771–776.
11. Yang, Y.J.; Liu, J.; Liu, F.; Wang, Z.; Miao, S. Molecular-level insights into mercury removal mechanism by pyrite. *J. Hazard. Mater.* **2018**, *344*, 104–112. [CrossRef] [PubMed]
12. Zhou, Z.J.; Liu, X.W.; Zhao, B.; Shao, H.Z.; Xu, Y.S.; Xu, M.H. Elemental mercury oxidation over manganese-based perovskite-type catalyst at low temperature. *Chem. Eng. J.* **2016**, *288*, 701–710. [CrossRef]
13. Díaz-Somoano, M.; Unterberger, S.; Hein, K.R. Mercury emission control in coal-fired plants: The role of wet scrubbers. *Fuel Process. Technol.* **2007**, *88*, 259–263. [CrossRef]

14. Li, B.; Wang, H.L. Effect of flue gas purification facilities of coal-fired power plant on mercury emission. *Energy Rep.* **2021**, *7*, 190–196. [CrossRef]
15. Li, H.; Wu, C.Y.; Li, Y.; Zhang, J.Y. CeO_2-TiO_2 catalysts for catalytic oxidation of elemental mercury in low-rank coal combustion flue gas. *Environ. Sci. Technol.* **2011**, *45*, 7394–7400. [CrossRef]
16. Fukuda, N.; Takaoka, M.; Doumoto, S.; Oshita, K.; Morisawa, S.; Mizuno, T. Mercury emission and behavior in primary ferrous metal production. *Atmos. Environ.* **2011**, *45*, 3685–3691. [CrossRef]
17. Zhao, S.J.; Mei, J.; Xu, H.M.; Liu, W.; Qu, Z.; Cui, Y. Research of mercury removal from sintering flue gas of iron and steel by the open metal site of Mil-101(Cr). *J. Hazard. Mater.* **2018**, *351*, 301–307. [CrossRef] [PubMed]
18. Yang, H.Q.; Xu, Z.H.; Fan, M.H.; Bland, A.E.; Judkins, R.R. Adcatalyst for capturing mercury in coal-fired boiler flue gas. *J. Hazard. Mater.* **2007**, *146*, 1–11. [CrossRef]
19. Scala, F. Simulation of mercury capture by activated carbon injection in incinerator flue gas in-duct removal. *Environ. Sci. Technol.* **2001**, *35*, 4367–4372. [CrossRef]
20. Chen, W.M.; Pei, Y.; Huang, W.J.; Qu, Z.; Hu, X.F.; Yan, N.Q. Novel effective catalyst for elemental mercury removal from coal-fired flue gas and the mechanism investigation. *Environ. Sci. Technol.* **2016**, *50*, 2564–2572. [CrossRef]
21. Yuan, Y.; Zhang, J.Y.; Li, H.L.; Li, Y.; Zhao, Y.C.; Zheng, C.G. Simultaneous removal of SO_2, NO and mercury using TiO_2-aluminum silicate fiber by photocatalysis. *Chem. Eng. J.* **2012**, *192*, 21–28. [CrossRef]
22. Wu, J.; Xu, K.; Liu, Q.Z.; Ji, Z.; Qu, C.; Qi, X.M. Controlling dominantly reactive (010) facets and impurity level by in-situ reduction of $BiOIO_3$ for enhancing photocatalytic activity. *Appl. Catal. B* **2018**, *232*, 135–145. [CrossRef]
23. Pavlish, J.H.; Sondreal, E.A.; Mann, M.D.; Olson, E.S.; Galbreath, K.C.; Laudal, D.L. Status review of mercury control options for coal-fired power plants. *Fuel Process. Technol.* **2003**, *82*, 89–165. [CrossRef]
24. Xu, H.M.; Qu, Z.; Zong, C.X.; Quan, F.Q.; Mei, J.; Yan, N.Q. Catalytic oxidation and adsorption of Hg^0 over low-temperature NH_3-SCR $LaMnO_3$ perovskite oxide from flue gas. *Appl. Catal. B* **2016**, *186*, 30–40. [CrossRef]
25. Cai, J.; Shen, B.X.; Li, Z.; Chen, J.H.; He, C. Removal of elemental mercury by clays impregnated with KI and KBr. *Chem. Eng. J.* **2014**, *241*, 19–27. [CrossRef]
26. He, C.; Shen, B.X.; Chen, J.H.; Cai, J. Adsorption and oxidation of elemental mercury over Ce-MnO_x/Ti-PILCs. *Environ. Sci. Technol.* **2014**, *48*, 7891–7898. [CrossRef]
27. Ding, F.; Zhao, Y.C.; Mi, L.L.; Li, H.L.; Li, Y.; Zhang, J.Y. Removal of gas-phase elemental mercury in flue gas by inorganic chemically promoted natural mineral catalyst. *Ind. Eng. Chem. Res.* **2012**, *51*, 3039–3047. [CrossRef]
28. Li, H.L.; Zhang, M.G.; Zhu, L.; Yang, J.P. Stability of mercury on a novel mineral sulfide sorbent used for efficient mercury removal from coal combustion flue gas. *Environ. Sci. Pollut. Res.* **2018**, *25*, 28583–28593. [CrossRef]
29. Takagi, M.; Kawai, T.; Soma, M.; Onishi, T.; Tamaru, K. The mechanism of the reaction between NO_x and NH_3 on V_2O_5 in the presence of oxygen. *J. Catal.* **1977**, *50*, 441–446. [CrossRef]
30. Zhao, L.K.; Li, C.T.; Zhang, J.; Zhang, X.N.; Zhan, F.M.; Ma, J.F. Promotional effect of CeO_2 modified support on V_2O_5–WO_3/TiO_2 catalyst for elemental mercury oxidation in simulated coal-fired flue gas. *Fuel* **2015**, *153*, 361–369. [CrossRef]
31. Lee, W.; Bae, G.N. Removal of elemental mercury (Hg^0) by nanosized V_2O_5/TiO_2 catalysts. *Environ. Sci. Technol.* **2009**, *43*, 1522–1527. [CrossRef] [PubMed]
32. Zhang, X.P.; Li, Z.F.; Wang, J.X.; Tan, B.J.; Cui, Y.Z.; He, G.H. Reaction mechanism for the influence of SO_2 on Hg^0 adsorption and oxidation with Ce-0.1-Zr-MnO_2. *Fuel* **2017**, *203*, 308–315. [CrossRef]
33. Zhang, A.C.; Xing, W.B.; Zhang, Z.H.; Meng, F.M.; Liu, Z.C.; Xiang, J. Promotional effect of SO_2 on CeO_2-TiO_2 material for elemental mercury removal at low temperature. *Atmos. Pollut. Res.* **2016**, *7*, 895–902. [CrossRef]
34. Yang, Z.Q.; Li, H.L.; Liu, X.; Li, P.; Yang, J.P.; Lee, P.H. Promotional effect of CuO loading on the catalytic activity and SO_2 resistance of MnO_x/TiO_2 catalyst for simultaneous NO reduction and Hg^0 oxidation. *Fuel* **2018**, *227*, 79–88. [CrossRef]
35. Wang, J.W.; Shen, Y.Y.; Dong, Y.J.; Qin, W.; Zhang, Q.P.; Lu, L.; Zhang, Y.G. Oxidation and adsorption of gas-phase Hg^0 over a V_2O_5/AC catalyst. *RSC Adv.* **2016**, *6*, 77553–77557. [CrossRef]
36. Zhang, Q.P. Removal of Hg^0 from Simulated Flue Gas by CuO/PG and V_2O_5/PG. Master's Thesis, Anqing Normal University, Anqing, China, 2018. (In Chinese)
37. Zhu, Y.C.; Han, X.J.; Huang, Z.G.; Hou, Y.Q.; Guo, Y.; Wu, M.H. Superior activity of CeO_2 modified V_2O_5/AC catalyst for mercury removal at low temperature. *Chem. Eng. J.* **2018**, *337*, 741–749. [CrossRef]
38. Ma, Y.P.; Mu, B.L.; Yuan, D.L.; Zhang, H.Z.; Xu, H.M. Design of MnO_2/CeO_2-MnO_2 hierarchical binary oxides for elemental elemental mercury removal from coal-fired flue gas. *J. Hazard. Mater.* **2017**, *333*, 186–193. [CrossRef]
39. Ye, D.; Wang, X.X.; Wang, R.X.; Wang, S.Y.; Liu, H.; Wang, H.N. Recent advances in MnO_2-based adsorbents for mercury removal from coal-fired flue gas. *J. Environ. Chem. Eng.* **2021**, *9*, 105993. [CrossRef]
40. Zhu, Y.C.; Hou, Y.Q.; Wang, J.W.; Guo, Y.P.; Huang, Z.G.; Han, X.J. Effect of SCR atmosphere on the removal of Hg^0 by a V_2O_5–CeO_2/AC catalyst at low temperature. *Environ. Sci. Technol.* **2019**, *53*, 5521–5527. [CrossRef]
41. Li, H.L.; Wu, C.Y.; Li, Y.; Li, L.Q.; Zhao, Y.C.; Zhang, J.Y. Role of flue gas components in mercury oxidation over TiO_2 supported MnO_x-CeO_2 mixed-oxide at low temperature. *J. Hazard. Mater.* **2012**, *243*, 117–123. [CrossRef]
42. He, C.; Shen, B.X.; Li, F.K. Effects of flue gas components on removal of elemental mercury over Ce–MnOx/Ti-PILCs. *J. Hazard. Mater.* **2016**, *304*, 10–17. [CrossRef] [PubMed]

43. Wang, Y.Y.; Shen, B.X.; He, C.; Yue, S.J.; Wang, F.M. Simultaneous removal of NO and Hg^0 from flue gas over Mn-Ce/Ti-PILCs. *Environ. Sci. Technol.* **2015**, *49*, 9355–9363. [CrossRef]
44. Zhao, L.K.; Li, C.T.; Li, S.H.; Wang, Y.; Zhang, J.Y.; Wang, T. Simultaneous removal of elemental mercury and NO in simulated flue gas over V_2O_5/ZrO_2-CeO_2 catalyst. *Appl. Catal. B* **2016**, *198*, 420–430. [CrossRef]
45. Morris, E.A.; Kirk, D.W.; Jia, C.Q.; Morita, K. Roles of sulfuric acid in elemental mercury removal by activated carbon and sulfur-impregnated activated carbon. *Environ. Sci. Technol.* **2012**, *46*, 7905–7912. [CrossRef] [PubMed]
46. Zhou, Q.; Duan, Y.F.; Chen, M.M.; Liu, M.; Lu, P. Studies on mercury adsorption species and equilibrium on activated carbon surface. *Energy Fuels* **2017**, *31*, 14211–14218. [CrossRef]
47. Rumayor, M.; Diaz-Somoano, M.; López-Antón, M.A. Temperature programmed desorption as a tool for the identification of mercury fate in wet-desulphurization systems. *Fuel* **2015**, *148*, 98–103. [CrossRef]
48. Ranea, V.A. A DFT + U study of H_2O adsorption on the V_2O_5(0 0 1) surface including van der Waals interactions. *Chem. Phys. Lett.* **2019**, *730*, 171–178. [CrossRef]